applied sciences

MDPI

Article

Mechanistic Studies of Hydrogen Evolution Reaction on Donor-Acceptor Conjugated Polymer Photocatalysts

Yves Ira A. Reyes [1,2], Li-Yu Ting [3], Xin Tu [2], Hsin-Yi Tiffany Chen [1,*], Ho-Hsiu Chou [3,*] and Carmine Coluccini [4,*]

1 Department of Engineering and System Science, National Tsing Hua University, Hsinchu 30013, Taiwan; yvesreyes@gapp.nthu.edu.tw
2 Department of Electrical Engineering and Electronics, University of Liverpool, Liverpool L69 3GJ, UK; xin.tu@liverpool.ac.uk
3 Department of Chemical Engineering, National Tsing Hua University No. 101, Sec. 2, Kuang-Fu Road, Hsinchu 30013, Taiwan; s107032528@m107.nthu.edu.tw
4 Institute of New Drug Development, China Medical University, No.91 Hsueh-Shih Road, Taichung 40402, Taiwan
* Correspondence: hsinyi.tiffany.chen@gapp.nthu.edu.tw (H.-Y.T.C.); hhchou@mx.nthu.edu.tw (H.-H.C.); carmine.coluccini@mail.cmu.edu.tw (C.C.); Tel.: +886-35715131 (ext. 34248) (H.-Y.T.C.); +886-35715131 (ext. 42508) (H.-H.C.); +886-04-2205-3366 (ext. 2534) (C.C.)

Received: 29 July 2020; Accepted: 30 September 2020; Published: 9 October 2020

Abstract: The application of donor-acceptor (D-A) conjugated polymer catalysts for hydrogen evolution reaction (HER) has shown great promise because of the tunability of such catalysts to have desired properties. Herein, we synthesized two polymer catalysts: poly[4,4′-(9-(4-aminophenyl)-9H-carbazole-3,6-diamine-*alt*-5-oxido-5-phenylbenzo[b]phosphindole-3,7-diyl)dibenzaldehyde] (PCzPO) and poly[N^1,N^1-bis(4-amino-2-fluorophenyl)-2-fluorobenzene-1,4-diamine-*alt*-5-oxido-5-phenylbenzo [b]phosphindole-3,7-diyl)dibenzaldehyde] (PNoFPO). The UV-vis absorption spectra showed that the less planar structure and the presence of electronegative fluorine atoms in the donor group of PNoFPO led to a higher optical gap compared to PCzPO, leading to almost five times faster HER rate using PCzPO compared to PNoFPO. However, density functional theory (DFT) calculations show that the frontier orbitals and the highest occupied molecular orbitals – lowest unoccupied molecular orbitals (HOMO-LUMO) gaps of PCzPO and PNoFPO D-A moiety models are very similar, such that, during light absorption, electrons move from donor to acceptor group where proton binding is preferred to happen thereafter. For both PCzPO and PNoFPO D-A moieties, H_2 formation through an intramolecular reaction with a barrier of 0.6–0.7 eV, likely occurs at the acceptor group atoms where protons bind through electrostatic interaction. The intermolecular reaction has nearly zero activation energy but is expected to occur only when the repulsion is low between separate polymers chains. Finally, experimental and DFT results reveal the importance of extended configurations of D-A polymers on HER rate.

Keywords: hydrogen evolution reaction; donor-acceptor conjugated polymer; density functional theory; optoelectronic properties; photocatalysis

1. Introduction

The conversion of solar energy into stored chemical energy is forefront research for the development of renewable energy [1]. On this note, hydrogen fuel (H_2) is known as the best fuel form because of its energy conversion efficiency and the fact that it can be generated from water and its oxidation only

produces water without any side products [2]. This motivates the search for photocatalyst materials for the photocatalysed hydrogen evolution reaction (HER) or water-splitting. Although inorganic materials are the current choice for photocatalysts, polymer photocatalysts are of great interest owing to their cheaper cost, sustainability and tunability [3]. Specifically, polymers made of alternating donor and acceptor units with highly conjugated structures have been shown to be more efficient photocatalysts for HER [4–9]. With this design, photoexcitation of electrons is accompanied by an intramolecular charge transfer from donor to acceptor groups [10]. This results in the accumulation of charge in the acceptor group, where efficient proton binding and reduction is expected to occur. By varying the donor and acceptor structure, the catalytic properties for HER can be controlled and improved.

Donor-acceptor type conjugated polymers have shown effective photocatalysis performance [11]. Recent designs used donor structures based on fluorene and triazine analogues [12–14]. The important aspect of successful catalysts seems to be the presence of high π conjugation and the introduction of heteroatoms. For instance, nitrogen and fluorine substitution on fluorene-based analogues have shown improved performance for HER associated with charge transfer efficiency [14]. However, the mechanism for binding of a proton, its reduction and formation of H_2 is still unclear. To understand how to design better D-A polymer photocatalysts for HER, it is important to understand how varying the structure affects the optoelectronic properties and the mechanism of HER to, in turn, get better HER performance. Density functional theory (DFT) calculations have been valuable towards this end. DFT has been used to predict the optoelectronic properties and photocatalytic efficiency of polymer photocatalysts [15,16]. Recently, the H^+ binding and H_2 formation mechanisms involved in HER using polymer photocatalysts have been studied by DFT as well [10,17].

In this work, we synthesised two novel polymer catalysts (Figure 1) with different donor units, aiming to compare their HER performance and understand their H_2 formation mechanisms. Both structures have the same phosphindole analogue acceptor unit, 4,4′-(5-oxido-5-phenylbenzo [b]phosphindole-3,7-diyl)dibenzaldehyde (PO). This acceptor structure features a phenylphosphine oxide group with a polar P = O moiety that has been associated with improved HER performance in previous studies [9,18]. A carbazole analogue, 9-(4-aminophenyl)-9H-carbazole-3,6-diamine (PCz), was used as a donor group for the first polymer while a fluorine substituted triphenylamine group, N^1,N^1-bis(4-amino-2-fluorophenyl)-2-fluorobenzene-1,4-diamine (PNoF) was used as a donor for the second. These polymers are herein referred to as PCzPO and PNoFPO, respectively. Their respective optoelectronic properties and HER rate were measured. We further performed DFT calculations to determine the frontier orbital density distributions and mechanism of the reaction to gain insight into this type of catalyst design. DFT results show that the molecular orbitals of the polymer structures allow for the expected intramolecular charge transfer, leading to efficient proton binding and reduction on acceptor groups, followed by forming of H_2 through an intramolecular reaction. The intermolecular reaction of forming H2 could take place only when the repulsion is low between polymers. Both experimental and DFT results indicate the importance of extended configurations of D-A polymers on HER performance.

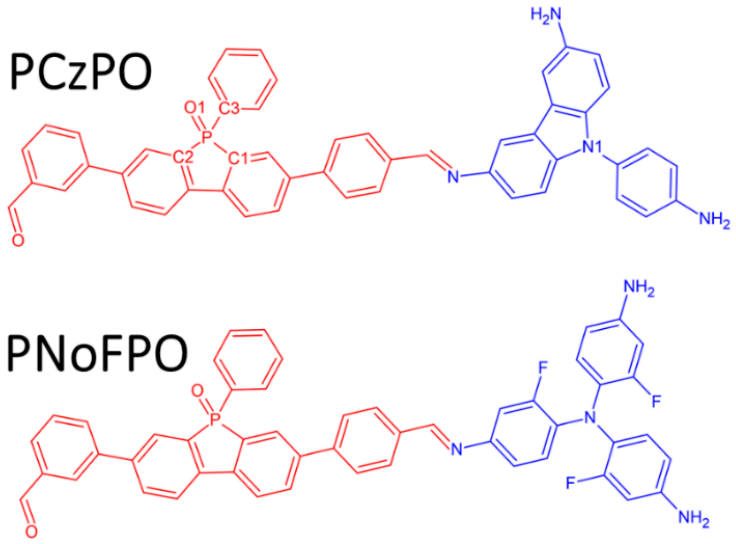

Figure 1. 2D molecular structures of poly[4,4′-(9-(4-aminophenyl)-9H-carbazole-3,6-diamine-*alt*-5-oxido-5-phenylbenzo[b]phosphindole-3,7-diyl)dibenzaldehyde] (PCzPO) and poly[N^1,N^1-bis(4-amino-2-fluorophenyl)-2-fluorobenzene-1,4-diamine-*alt*-5-oxido-5-phenylbenzo[b]phosphindole-3,7-diyl) dibenzaldehyde] (PNoFPO) donor-acceptor (D-A) moieties (donor group in blue and acceptor group in red).

2. Materials and Methods

2.1. General Method

All reagents were obtained from commercial suppliers and used without further purification. ^{1}H NMR spectra were measured using a Bruker Avance 500 MHz NMR spectrometer. Mass spectra were measured by a VARIAN 901-MS TQ-FT Mass Spectrometer. UV–vis absorption spectra of the polymers were recorded using Hitachi U-3300 spectrophotometers. The energy levels of the HOMOs were measured using a photoelectron spectrometer (model AC-2). Optical gaps were calculated from the onsets of the absorption spectra. The energy levels of the LUMO were calculated by subtracting the optical gap from the HOMO energy levels. Water for the H_2 evolution experiments was purified using an Elix UV.

2.1.1. Synthesis of 3,6-dinitro-9H-carbazole

$Cu(NO_3)_2{\cdot}2.5\ H_2O$ (14.5 g) was added into a mixture of acetic acid (25 mL) and acetic anhydride (50 mL) in a round bottle at room temperature. The mixture was stirred for 10 min, and then added carbazole (8.36 g) in. 25 mL of acetic acid was added afterwards. The mixture was stirred for 15 min and then poured into 500 mL water. The precipitate was collected by filtration and then dissolved in 100 mL KOH (20%). The solution was collected by filtration, and then 50 mL HCl (37%) was added into it to get precipitate. The precipitate was collected by filtration and washed by water. It was dried at 100 °C under vacuum. The yield was 8.0 g (52%). ^{1}H NMR (500 MHz, $CDCl_3$): δ 9.39 (d, J = 2 Hz, 2H), 8.43 (dd, J = 2 Hz, J = 9 Hz, 2H), 7.82 (d, J = 9 Hz, 2H).

2.1.2. Synthesis of 3,6-dinitro-9-(4-nitrophenyl)-9H-carbazole

3,6-dinitro-9H-carbazole (0.257g) and cesium fluoride were added into 0.155 g of 1-fluoro-4-nitrobenzene in a round bottle under nitrogen atmosphere. Dry DMF (4 mL) was added afterwards. The mixture was stirred at 150 °C under nitrogen for one day and then cooled to room temperature. It was poured into 50 mL solution (water:methanol = 1:1). The precipitate was collected by filtration and then successively washed with water, KOH (20%), and methanol. The solid was dried at 150 °C under vacuum. The yield was 0.26 g (crude product).

2.1.3. Synthesis of 9-(4-aminophenyl)-carbazole-3,6-diamine

3,6-dinitro-9-(4-nitrophenyl)-9H-carbazole (1.89 g), tin (2.97 g) and HCl (37%, 50 mL) were mixed in a round bottle and stirred at 100 °C for one day. It was cooled to room temperature and then poured into 250 mL NaOH (20%) in an ice bath. The precipitate was collected by filtration and then washed by water, dissolved in ethyl acetate (EA). The remaining water in the EA solution was removed by $MgSO_4$. The mixture was purified by column chromatography (EA). It was poured into hexane slowly. The precipitate was collected by filtration and then dried at 100 °C under vacuum. The yield was 0.67 g (47%). ^{1}H NMR (500 MHz, $CDCl_3$): δ 7.11 (d, J = 2 Hz, 2H), 7.07 (d, J = 8.5 Hz, 2H), 6.92 (d, J = 9 Hz, 2H), 6.72 (d, J = 8.5 Hz, 2H), 6.66 (dd, J = 2 Hz, J = 8.5 Hz, 2H), 5.23 (s, 2H), 4.65 (br, 4H). MS (ESI+): calculated 288.1375, found 289.1456.

2.1.4. Synthesis of tris(2-fluoro-4-nitrophenyl)amine

2-fluoro-4-nitroaniline (0.781 g), 1-bromo-2-fluoro-4-nitrobenzene (2.42 g), CuI (0.19 g), K_2CO_3 (4.14 g), L-proline (0.23 g), and tetrahydrofuran (THF) (50 mL) were mixed and stirred at 80 °C for one day. It was cooled to room temperature and then poured into 300 mL water. The precipitate was collected by filtration and then washed by water, dissolved in EA, and then dried by $MgSO_4$. The mixture was purified by column chromatography (hexane). The yield was 1.8 g (83%). ^{1}H NMR (500 MHz, $CDCl_3$): δ 7.98 (dd, J = 2.5 Hz, J = 8 Hz, 3H), 7.93 (dd, J = 1 Hz, J = 2.5 Hz, 3H), 7.76 (dd, J = 6.5 Hz, J = 9 Hz, 3H).

2.1.5. Synthesis of tris(2-fluoro-4-aminophenyl)amine

tris(2-fluoro-4-nitrophenyl)amine (1.736 g), tin (2.374 g), and HCl (37%, 40 mL) were mixed and stirred at 100 °C for 1 day. It was cooled to room temperature and then poured into 250 mL NaOH (20%) in an ice bath. The precipitate was collected by filtration and then washed by water and then dried under vacuum. The yield was 1.2 g (87%). ^{1}H NMR (500 MHz, $CDCl_3$): δ 7.22 (d, J = 8 Hz, 3H), 6.43 (dd, J = 2.5 Hz, J = 10.5 Hz, 3H), 6.33 (dd, J = 2.5 Hz, J = 9 Hz, 3H), 3.75 (br, 6H). MS (ESI+): calculated 344.1249, found 345.1510.

2.1.6. Synthesis of 4,4′-(5-oxido-5-phenylbenzo[b]phosphindole-3,7-diyl)dibenzaldehyde

3,7-dibromo-5-phenylbenzo[b]phosphindole 5-oxide (0.936 g), (4-formylphenyl)boronic acid (0.899 g), Na_2CO_3 (2.544 g), Tetra-n-butylammonium bromide (0.026 g), $Pd(PPh_3)_4$ (0.111 g) were mixed together and kept in N_2 atmosphere. Toluene (40 mL) and water (10 mL) were added afterwards. The mixture was stirred at 120 °C for 2 day and then cooled to room temperature. Product was extracted by EA. It was washed by ethanol and dried under vacuum. Yield was 0.2 g (20%). ^{1}H NMR (500 MHz, $CDCl_3$): δ 10.04 (s, 2H), 7.93–8.00 (m, 8H), 7.89 (td, J = 1.5 Hz, J = 8 Hz), 7.69–7.76 (m, 6H), 7.51 (t, J = 7 Hz), 7.41 (td, J = 7.5 Hz, J = 3 Hz, 2H).

2.1.7. Synthesis of PCzPO

4,4′-(5-oxido-5-phenylbenzo[b]phosphindole-3,7-diyl)dibenzaldehyde (0.145 g), acetic acid (0.607 g), 9-(4-aminophenyl)-carbazole-3,6-diamine (0.058 g), mesitylene 6 mL, and dioxane 6 mL were mixed and done freeze-pump-thaw method. The mixture was stirred at 120 °C, 0.1 atm for three days and then cooled to room temperature. It was washed by acetone and dried at 120 °C under vacuum for 12 h.

2.1.8. Synthesis of PNoFPO

4,4′-(5-oxido-5-phenylbenzo[b]phosphindole-3,7-diyl)dibenzaldehyde (0.145 g), acetic acid (0.607 g), tris(2-fluoro-4-aminophenyl)amine (0.069 g), mesitylene 6 mL, and dioxane 6 mL were mixed and done freeze-pump-thaw method. The mixture was stirred at 120 °C, 0.1 atm for three days

and then cooled to room temperature. It was washed by acetone and dried at 120 °C under vacuum for 12 h.

2.2. Hydrogen Evolution Experiments

The polymer powder (3 mg) and 90 μL H_2PtCl_6 (0.1 wt% in water) was added into the mixture (water, triethylamine, and methanol (1:1:1)) in a glass with a cool jacket, sealed by septum. The mixture was sonicated and degassed by Ar bubbling. The suspension was illuminated with 350 W Xe-lamp (1000 W/m^2, 380 nm–780 nm). Hydrogen samples were taken with a gas-tight syringe and injected in a Shimadzu GC-2014 gas chromatograph, with Ar as the carrier gas. Hydrogen was detected with a thermal conductivity detector, referring to the standard hydrogen gases with known concentrations. Increased pressure from the evolved hydrogen is neglected in the calculations.

2.3. Computational Details

All density functional calculations were conducted using the Gaussian16 package [19]. Three-dimensional models of the PCzPO and PNoFPO D-A moiety were built using Avogadro molecular editing software [20] and preoptimised using molecular mechanics forcefield (MMFF) [21]. Exchange and correlation were treated using the B3LYP hybrid functional, composed of 20% exact Hartree–Fock exchange [22]. Geometry optimisations were performed using the 6–31 g(d) basis set. Frequency analyses were performed to confirm that the optimised structures correspond to the true minimum in the potential energy surface. Single point energy and frequency calculations were then performed using the 6–311 g(d,p) basis set to calculate the Gibbs free energies. These computational approaches have been extensively used to study polymer photocatalysts and are shown to consistently reproduce experimental orbital energies at a reasonable computational cost [15,23–26]. The average proton binding free energies (ΔG_{H+}) were calculated as follows

$$\Delta G_{H+} = G_{H+/Polymer} - G_{Polymer} - (1/2)G_{H_2} \quad (1)$$

where $G_{H+/Polymer}$, $G_{Polymer}$, and G_{H_2} are the calculated Gibbs free energies of the protonated D-A moiety, the bare D-A moiety and the free hydrogen molecule, respectively. Finally, atomic charge distributions were calculated using the Mulliken population analysis.

3. Results and Discussions

3.1. Experimental Characterisation and HER Performance

In this study, we successfully synthesised PCzPO and PNoFPO via Schiff-base condensation. The polymers were poorly soluble in any solvent because of their large molecular weight. The polymers could only be dispersed in an aqueous solution as a suspension. We examined the photophysical properties of both polymers, using UV-vis absorption and photoelectron spectroscopy. The two polymers showed strong absorption bands around 330–337 nm, as summarised in Table 1. The onset of UV-vis absorption of PNoFPO was blue-shifted (Figure S1), compared to that of PCzPO, due to the electronegative fluorine substitution at the ortho sites of the donor group [27,28], bringing about a larger optical gap (3.03 eV in Table 1). Higher planarity of PCzPO with more extended π conjugation and more propensity to stack together led to a narrower optical gap (2.74 eV in Table 1).

Table 1. UV-vis absorption peaks, HOMO/LUMO energy levels, optical gap and hydrogen evolution rate (HER rate) using PCzPO and PNoFPO D-A polymers.

Polymer	Absorption Peaks [nm]	HOMO/LUMO [eV] [a,b]	Optical Gap [eV] [c]	HER Rate [μmol h^{-1} g^{-1}] [d]
PCzPO	334, 357	−5.59/−2.85	2.74	34.23
PNoFPO	342, 368	−5.87/−2.84	3.03	7.34

[a] HOMO was measured by a photoelectron spectrometer (model AC-2). [b] LUMO was calculated by HOMO + Optical gap. [c] calculated from UV-vis absorption. [d] 3 mg polymer in 10 mL mixture (water, triethylamine, and methanol (1:1:1)). 3 wt% H_2PtCl_6 was added.

Next, we added the polymers into an aqueous mixture and tested the hydrogen evolution performance. Ar was chosen as bubbling gas because there was no hydrogen evolution using N_2 atmosphere. It showed that the hydrogen evolution rate of PCzPO was almost five times that of PNoFPO. This could be explained by the lower optical gap of PCzPO, resulting in more opportunities to absorb light energy for HER. Other factors, such as solubility [29,30] and reaction mechanism [17] might also affect HER performance. In the proceeding sections, we specifically analyse their frontier molecular orbitals and explore HER mechanisms using DFT calculations.

3.2. Density Functional Theory Calculations

To simplify the polymer models and exclude complicated configuration effects, we used a single PCzPO and PNoFPO D-A moiety for DFT calculations. We analysed their electron density distribution of molecular orbitals, their free energy of proton binding and their free energy of activation for both intramolecular and intermolecular H_2 formation, demonstrated in previous studies [10,17,26].

We computed the difference between the energies of the highest occupied molecular orbital (HOMO) and lowest unoccupied molecular orbital (LUMO) to predict the capability of the polymer to absorb photons as photocatalysts. The DFT calculated HOMO-LUMO gaps (Figure 2) for PCzPO (2.48 eV) and PNoFPO (2.42 eV) are inconsistent from the measured experimental optical gaps listed in Table 1. In general, the experimental optical gap, which is a better indicator of photon absorption efficiency normally differs from the HOMO-LUMO gap by an amount called the exciton binding energy [31]. In addition, realistic extended chains of polymers might affect HOMO-LUMO gaps due to extended π conjugation and interchain stacking or clustering, which were not taken into consideration in our simulation model.

In the donor-acceptor type conjugated polymer, the photoexcitation of the electron in the orbital (HOMO) involves an intramolecular charge transfer from the donor group to the acceptor group. To demonstrate this, the electron density distributions of the frontier orbitals of both polymers were analysed and shown in Figure 2. For both PCzPO and PNoFPO, the electron density for high-lying occupied molecular orbitals is concentrated on the donor group while that of the low-lying unoccupied molecular orbitals is concentrated on the acceptor group. Thus, when the electrons in the HOMO is excited to the LUMO, the electron is indeed transferred from the donor group to the acceptor group.

Photocatalytic HER involves (i) the photoexcitation of the neutral polymer catalyst (P), (ii) the electron transfer from a sacrificial donor to P, (iii) the proton (H^+) binding to P and (iv) the reduction of the H^+ and the formation of hydrogen (H_2) and recovery of P. Although the actual order of the first three steps is not very clear, we assume herein that the first two steps happen before the proton binding. Figure 3 shows the schematic representation of the first two steps culminating in the formation of an anion radical intermediate form ($P^{\bullet-}$) of the polymer catalyst. To justify this assumption, we compared the binding free energy of a proton (ΔG_{H+}) to the phosphorous oxide of the neutral catalysts and the reduced catalysts. Predictably so, the binding free energies of H^+ to the reduced polymers (2.96 and 3.02 eV) were almost twice as thermodynamically favourable than those to the neutral polymers (5.93 and 5.95 eV) for PCZPO and PNoFPO D-A moiety, respectively (in Table 2). This makes it reasonable to assume that the formation of the unstable $P^{\bullet-}$ precedes the binding of H^+ and may be the driving

force for faster H^+ binding and overall HER. Thus, in contrast to previous theoretical calculations that bind H^+ to the neutral catalyst, P [10,26], the proceeding calculations in this work goes with the assumption that H^+ binds to $P^{\bullet-}$. Furthermore, due to the accumulation of electrons in the acceptor group, as explained above, H^+ will most probably bind to the negatively charged acceptor group atoms due to electrostatic interaction. In addition, the similar proton binding free energies to P or $P^{\bullet-}$ correlate with the similar LUMO levels of PCZPO and PNoFPO D-A moieties.

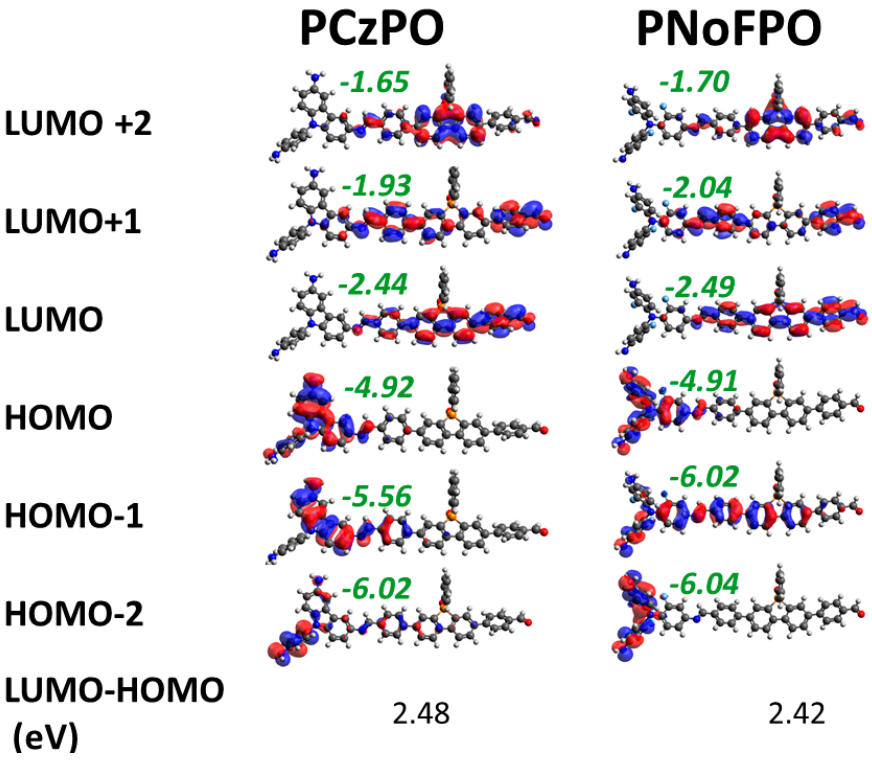

Figure 2. 3D electron density distribution of the frontier orbitals of PCzPO and PNoFPO D-A moieties, computed at the B3LYP/6-311G(d,p) level of theory. Energy levels (eV) of each orbital is shown in green, and the HOMO-LUMO gaps are shown at the bottom of each column.

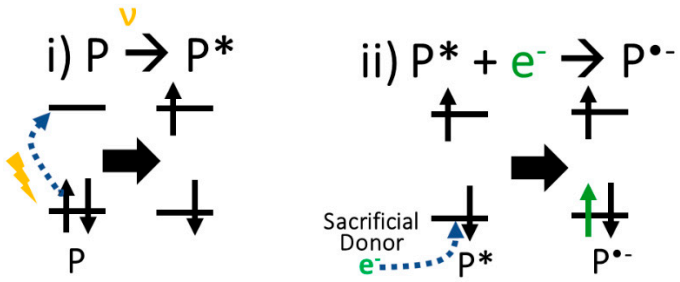

Figure 3. Schematic representation of the formation of $P^{\bullet-}$.

Table 2. Proton binding free energy (ΔG_H) for neutral and negative PCZPO and PNoFPO D-A moieties with H bound to the O atoms of PO groups of acceptor groups, computed by density functional theory (DFT).

Polymer Catalyst	Proton Binding Free Energy (eV)	
	$P + H^+ \rightarrow PH^+$	$P^{\bullet-} + H^+ \rightarrow PH$
PCzPO	5.93	2.96
PNoFPO	5.95	3.02

The frontier molecular orbitals (in Figure 2) show that H^+ might bind to acceptor atoms where photoexcited electrons are localised. Since PCzPO performed better in the experiment, we began with the PCzPO for a detailed exploration of H^+ binding and H_2 formation mechanisms. First, the frontier molecular orbitals of the $PCzPO^{\bullet-}$ before and after protonation were analysed and depicted in Figure 4. The HOMO of $PCzPO^{\bullet-}$ was similar to the LUMO of the neutral PCzPO (first column in Figure 2), except for the increased energy levels brought by spin and charge destabilisation and the new HOMO containing the radical corresponds to the LUMO of the neutral PCzPO. The H^+ binding neutralises the excess charge, which makes the molecular orbital energy levels of $H\text{-}PCzPO^{\bullet}$ lower compared to $PCzPO^{\bullet-}$. In addition, the frontier molecular orbitals of neutral PCzPO and $H\text{-}PCzPO^{\bullet}$ were similar, apart from the HOMO–2 molecular orbital. For $H\text{-}PCzPO^{\bullet}$, the electron density was concentrated on the phosphindole group to which the proton was bound. This was a new orbital formed through the interaction with the bound H^+. Figure 5 shows the simplified molecular orbital diagram, which summarises the transfer of electron observed in Figure 4. The incoming H^+ interacted with the HOMO of $PCzPO^{\bullet-}$ to form $H\text{-}PCzPO^{\bullet}$, where a new bonding orbital contributed by the H atom was formed. This is a simplified interpretation since it is possible for orbitals to mix and many different molecular orbitals to interact with H^+. But what is important is that H^+ gained electron density while the LUMO of PCzPO (HOMO of $PCzPO^{\bullet-}$) became empty again. Thus, there is a clear electron transfer from the donor group atoms to the bound H^+.

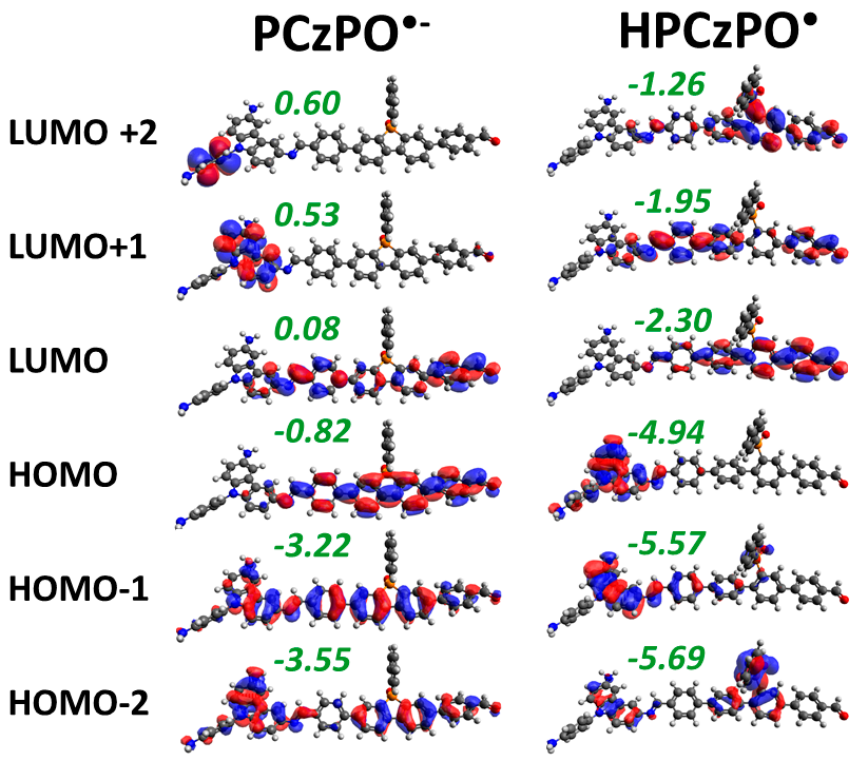

Figure 4. 3D electron density distribution of the frontier orbitals of $PCzPO^{\bullet-}$ and $H\text{-}PCzPO^{\bullet}$ calculated under DFT-B3LYP/6-311G(d,p) level of theory.

The Mulliken charge of $PCzPO^{\bullet-}$ was analysed to explore the various possible H^+ binding sites. The most negatively charged atoms of PCzPO were labelled accordingly in Figure 1 and listed in Table 3. In a previous DFT study of D-A polymers [10], electronegative heteroatoms were assumed as binding sites due to charge considerations. However, as seen in Table 3, even though N1 was one of the most negatively charged atoms, the H^+ binding to this site is the least favourable. This is because N1 is part of the donor PO group where the HOMO of $PCzPO^{\bullet-}$ intermediate has no electron density. Thus, we posit that besides overall electron density, the electron density of the HOMO is crucial in

predicting H^+ binding sites and further support the deduction of H^+ being expected to bind to atoms of the acceptor group in a donor-acceptor type conjugated polymer.

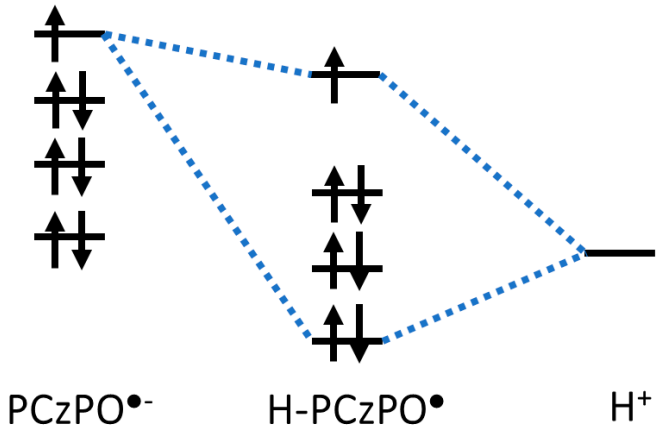

Figure 5. Molecular orbital diagram of the binding of a proton to $PCzPO^{\bullet-}$.

Table 3. Mulliken charge analysis and H^+ binding free energy (ΔG_{H+}) of different binding sites and configurations on $PCZPO^{\bullet-}$ moiety, computed by DFT.

Site	Configuration	Mulliken Charge	ΔG_{H+} (eV)
C1	a	−0.417	2.83
	b		2.98
C2	a	−0.412	2.90
	b		2.99
C3		−0.382	3.07
O		−0.593	2.97
N1		−0.593	4.37

Since phosphorous is the least electronegative atom for the polymer catalyst, atoms directly bonded to it become negatively charged due to induction, making them preferred sites for H^+ binding. As depicted in Figure 1, the phosphorous atom of the P = O group is bonded to 3 carbon atoms (C1 to C3) and an oxygen atom (O). C1 and C2 are the carbons of the phosphindole group with C2 being close to the acceptor group while C3 is the carbon of the phenyl group. Table 3 shows that H^+ bound more strongly to C1 and C2 than to O. The binding of H^+ to C1 and C2 led to various possible configurations, as shown in Figure 6. The more stable configurations, C1a and C2a, were generated when H^+ binds from the top, along the plane of the phosphole ring. In this configuration, the bond of C1 or C2 to the phosphorous was broken to open up the phosphole ring. This allows the C1 or C2 to maintain sp^2 hybridisation and maintain the extended π conjugation of the molecule. But H^+ may also bind perpendicular to the plane of the phosphole ring (C1b and C2b in Figure 6). This does not break the bond to phosphorous but is less stable because it converts the carbon binding site to an sp^3 hybridised tetrahedral centre, thus, breaking the planar configuration of the ring and interrupting the π conjugation. We note that the difference in H^+ binding energies for proton binding onto the three C and the O site was very small (<0.2 eV) as seen in Table 3. This means that the H^+ may realistically bind to any of these sites to form $H\text{-}PCZPO^{\bullet}$. In fact, H^+ may very well bind to sites other than the ones discussed here since the charges of the C atoms along the P = O acceptor group (not shown here) did not differ significantly. However, for practicality, we proceeded with the assumption that these sites are the most probable H^+ binding sites.

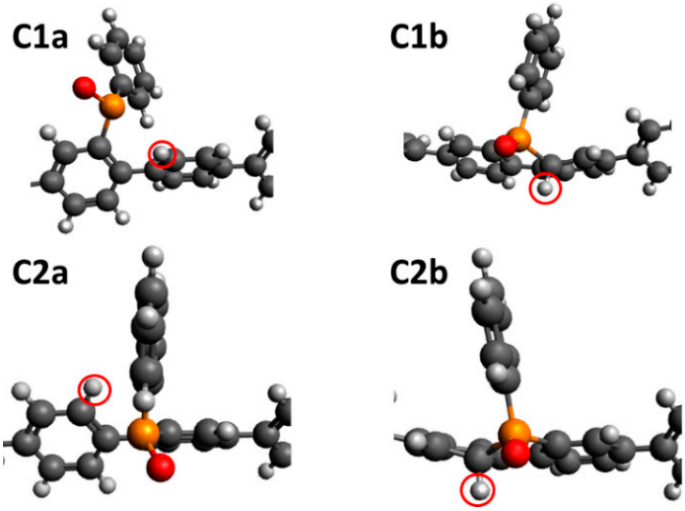

Figure 6. Possible configurations of proton binding onto C1 and C2.

To study the last step of the hydrogen evolution reaction where H_2 is finally formed and the initial neutral polymer is recovered, two possible reaction mechanisms were considered. In an intramolecular reaction mechanism, a single P-H$^\bullet$ will undergo the above-described protonation process again and bind another proton in a different site to form an H2-PCzPO intermediate before releasing the product: P-H_2 → P + H_2. In an intermolecular mechanism, two H-PCZPO$^\bullet$ molecules will react to form the hydrogen molecule: 2 P-H → 2 P + H_2. The minimum energy paths (MEP) of these two reaction mechanisms were calculated.

In an intramolecular reaction mechanism, the P-H$^\bullet$ molecule would be reduced and protonated for a second time to form a P-H_2 intermediate. For simplicity, it was assumed, based on the results discussed above, that the first proton would bind to C1. As shown in Figure 7, two possible P-H_2 states were then considered leading to two possible intramolecular mechanisms: (i) the second H+ binds to C2 (C1-H-C2-H) and (ii) the second H^+ binds to O (C1-H-O-H). C1-H-C2-H was more stable compared to C1-H-O-H. However, this results in the higher activation energy for the C1-H-C2-H pathway (E_a = 1.16 eV, black line in Figure 7) compared to the C1-H-O-H mechanism (E_a = 0.66 eV, the red line in Figure 7). This means that the H_2 formation would proceed faster through the C1-H-O-H mechanism from a kinetic perspective. Thus, H_2 formation on PCzPO will likely proceed through an intramolecular mechanism after overcoming the barrier of 0.66 eV. We also elucidated the intramolecular H_2 formation using PNoFPO to show that PNoFPO indeed generated a very similar reaction coordinate and barrier (0.61 eV) to PCzPO moiety (Figure S3).

To study the intermolecular mechanism, a reaction between two molecules of H-PCzPO$^\bullet$ with the most stable configuration, C1a (ΔG_H = 2.83 eV), was initially chosen as the starting structure. However, the optimisation of two H-PCzPO$^\bullet$ moieties with C1a configurations led to the formation of a phosphorous-phosphorous bond which inhibited the interaction of the H atoms and H_2 formation (Figure S4). Because of this, C1b configuration was chosen as a starting structure to find the MEP for the formation of H_2. The calculated reaction coordinate for this mechanism (Figure 8) shows a hydrogen formation reaction with activation energy (E_a) equal to zero. This implies a barrierless and spontaneous ($\Delta G = -0.116$) formation of H_2 through this intermolecular reaction mechanism. However, it is important to note that the two P-H molecules needed to be oriented such that the hydrogens involved in the reaction are closely pointed to each other, implying that intermolecular H_2 formation is only likely to occur when the repulsion between polymers is low. The higher HER rate from the higher molecular stacking of PCzPO polymers might be possibly due to the higher possibility of forming H_2 via an intermolecular reaction mechanism.

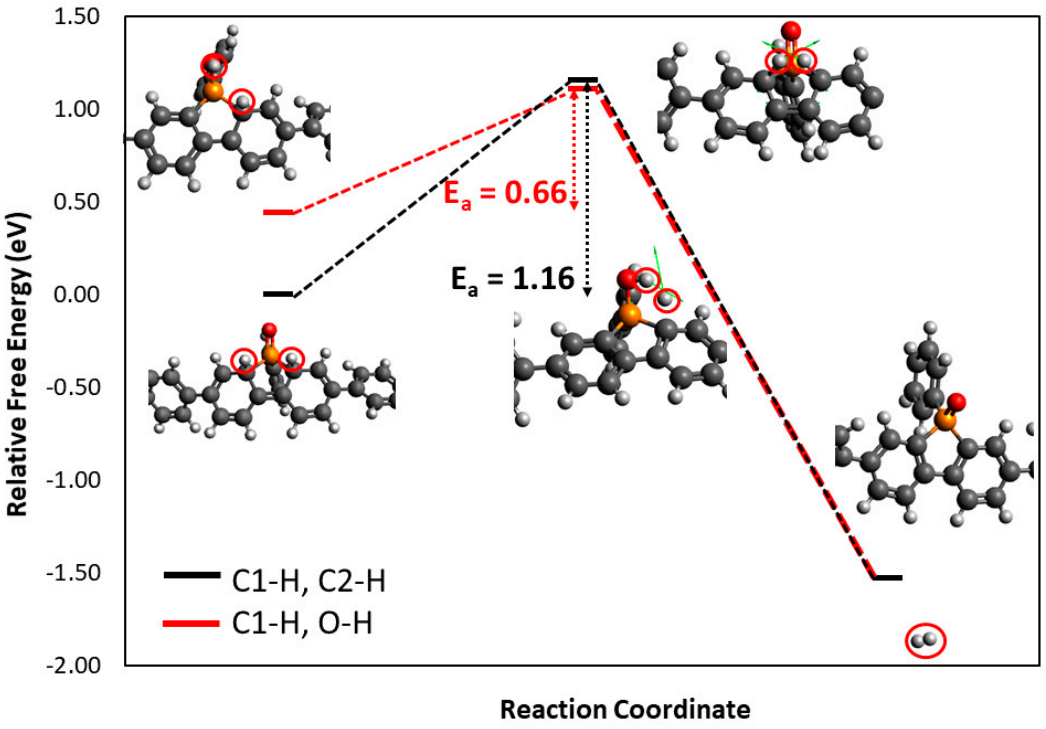

Figure 7. Energy diagram of intramolecular H_2 formation using the PCzPO D-A moiety model protonated at C1 and C2 (red line) and C1 and O (black line), computed by DFT.

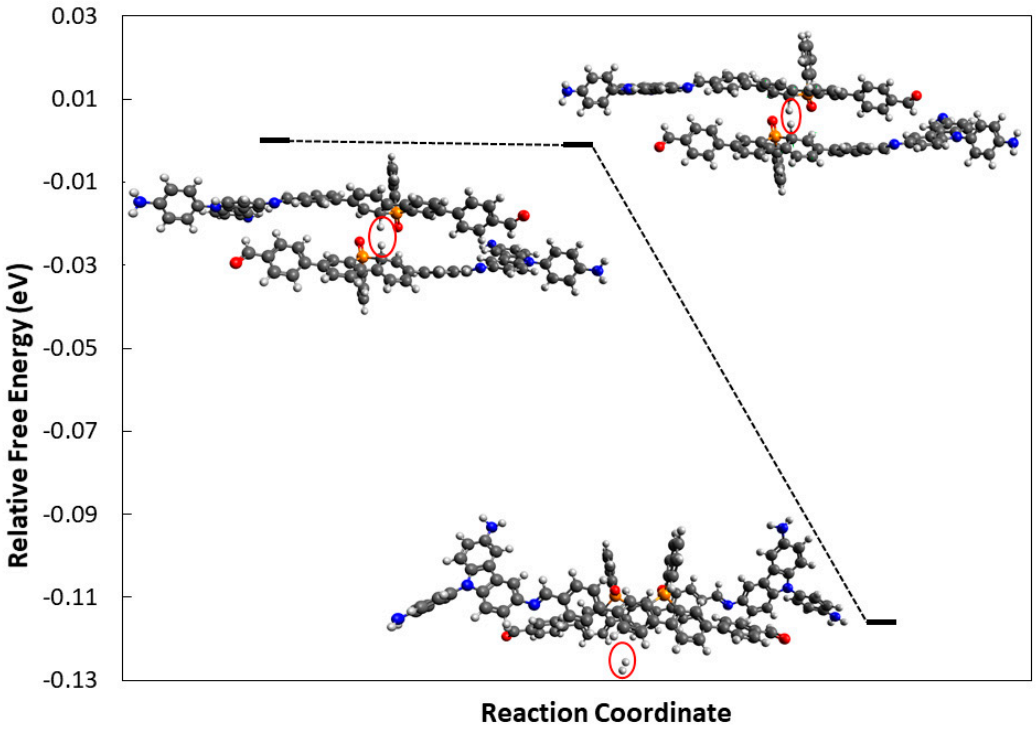

Figure 8. Energy diagram of intermolecular H_2 formation using two protonated PCzPO D-A moiety models, computed by DFT.

4. Conclusions

In this work, we have successfully synthesised two novel donor-acceptor (D-A) type conjugated polymer photocatalysts, PCzPO and PNoFPO. Optoelectronic properties of the polymers were

characterised both experimentally and using density functional theory calculations. From the perspective of electronic structures, the measured optical gap of PCzPO was lower than that of PNoFPO by UV-vis absorption, which is inconsistent with the similar HOMO-LUMO gaps of PCzPO and PNoFPO D-A moieties, computed by DFT. This discrepancy might be associated with better-extended π conjugation and potential intermolecular stacking brought about by the more planar nature of the carbazole group of PCzPO compared to the triphenylamine group of PNoFPO; these structural effects were not considered in DFT D-A moiety models. Because of the intermolecular stacking of carbazole groups, leading to longer conjugation and higher electron transporting capability, PCzPO outperformed PNoFPO in HER performance. Further DFT analysis of the PCzPO model was then performed to investigate the details of H^+ binding, reduction and H_2 evolution mechanisms. First, it shows that the more natively charged C and O atoms of the phosphindole analogue acceptor group are the primary protonation sites. Secondly, we deduce that H_2 formation is likely taken place through an intramolecular reaction with similar activation energies of 0.6–0.7 eV for both PCzPO and PNoFPO. Though the intermolecular reactions to form H_2 is almost barrierless, this pathway is expected to occur when the repulsion between polymers is low. Presumably, the higher intermolecular stacking of PCzPO D-A polymers leads to a higher possibility of occurrence of intermolecular H_2 formation. Finally, from our experimental and DFT results, we highlight that the extended configurations of D-A conjugated polymers could be the crucial factor leading to higher HER rate while the donor structure determines the mechanisms involved in transforming H^+ to H_2. The detailed electron push-pull interactions of adding heteroatoms in either acceptor or donor groups on HER performance will be studied in the future.

Supplementary Materials: The following are available online at http://www.mdpi.com/2076-3417/10/20/7017/s1, Figure S1: UV-vis absorption spectra of PCzPO and PNoFPO D-A polymer, measured in Dicholoromethane Figure S2: Hydrogen evolution profile of PCzPO and PNoFPO using visible light for polymers (5 mg catalyst in 10 mL mixture (water: MeOH: triethylamine = 1:1:1), 1000 W/m^2, 380 nm–780 nm, 90 µL H_2PtCl_6 (1M) was added). Figure S3: Energy diagram of intramolecular H_2 formation using PCzPO (left) and PNoFPO (right) D-A moiety models, computed by DFT. Figure S4: Formation of a phosphorous-phosphorous bond (P atoms are shown as orange spheres and the bond is shown as an orange line) preventing the interaction of bound H atoms (highlighted in light blue) for a complete hydrogen evolution, computed by DFT.

Author Contributions: Conceptualisation, Y.I.A.R., H.-H.C. and H.-Y.T.C.; formal analysis, Y.I.A.R. and L.-Y.T.; funding acquisition, H.-Y.T.C., H.-H.C. and C.C.; methodology, Y.I.A.R., L.-Y.T., H.-Y.T.C., H.-H.C. and C.C.; resources, H.-Y.T.C. and H.-H.C.; software, H.-Y.T.C.; supervision, H.-Y.T.C., H.-H.C. and C.C.; validation, Y.I.A.R.; writing—original draft, Y.I.A.R. and L.-Y.T.; writing—review and editing, Y.I.A.R., X.T., H.-Y.T.C., H.-H.C. and C.C. All authors have read and agreed to the published version of the manuscript.

Funding: H.-Y.T.C. acknowledges the financial support provided by the Ministry of Science and Technology (MOST) (108-2112-M-007-023-MY3 and 109-3116-F-007-001) and National Tsing Hua University grants (109Q2716E1), and the computing resource of TAIWANIA in National Center for High-Performance Computing (NCHC) in Taiwan. H.-H.C. is grateful for the support of MOST—MOST 109-2636-E-007-021. C.C. thanks the financial support by MOST-107-2113-M-039-008-MY3. Y.I.A.R., X.T. and H.-Y.T.C. acknowledge the dual PhD degree programme between the National Tsing Hua University and the University of Liverpool.

Conflicts of Interest: The authors declare no conflict of interest.

References

1. Tachibana, Y.; Vayssieres, L.; Durrant, J.R. Artificial photosynthesis for solar water-splitting. *Nat. Photonics* **2012**, *6*, 511–518. [CrossRef]
2. Jain, A.; Shin, Y.; Persson, K.A. Computational predictions of energy materials using density functional theory. *Nat. Rev. Mater.* **2016**, *1*, 15004. [CrossRef]
3. Jayakumar, J.; Chou, H. Recent advances in visible-light-driven hydrogen evolution from water using polymer photocatalysts. *ChemCatChem* **2020**, *12*, 689–704. [CrossRef]
4. Yuan, J.; Zhang, Y.; Zhou, L.; Zhang, G.; Yip, H.L.; Lau, T.K.; Lu, X.; Zhu, C.; Peng, H.; Johnson, P.A.; et al. Single-junction organic solar cell with over 15% efficiency using fused-ring acceptor with electron-deficient core. *Joule* **2019**, *3*, 1140–1151. [CrossRef]

5. Zhou, N.; Dudnik, A.S.; Li, T.I.N.G.; Manley, E.F.; Aldrich, T.J.; Guo, P.; Liao, H.C.; Chen, Z.; Chen, L.X.; Chang, R.P.H.; et al. All-polymer solar cell performance optimized via systematic molecular weight tuning of both donor and acceptor polymers. *J. Am. Chem. Soc.* **2016**, *138*, 1240–1251. [CrossRef]
6. Benten, H.; Mori, D.; Ohkita, H.; Ito, S. Recent research progress of polymer donor/polymer acceptor blend solar cells. *J. Mater. Chem. A* **2016**, *4*, 5340–5365. [CrossRef]
7. Tseng, P.J.; Chang, C.L.; Chan, Y.H.; Ting, L.Y.; Chen, P.Y.; Liao, C.H.; Tsai, M.L.; Chou, H.H. Design and synthesis of cycloplatinated polymer dots as photocatalysts for visible-light-driven hydrogen evolution. *ACS Catal.* **2018**, *8*, 7766–7772. [CrossRef]
8. EL-Mahdy, A.F.M.; Elewa, A.M.; Huang, S.; Chou, H.; Kuo, S. Dual-function fluorescent covalent organic frameworks: HCl sensing and photocatalytic H_2 evolution from water. *Adv. Opt. Mater.* **2020**, 2000641. [CrossRef]
9. Wang, W.H.; Ting, L.Y.; Jayakumar, J.; Chang, C.L.; Lin, W.C.; Chung, C.C.; Elsayed, M.H.; Lu, C.Y.; Elewa, A.; Chou, H.H.; et al. Design and synthesis of phenylphosphine oxide-based polymer photocatalysts for highly efficient visible-light-driven hydrogen evolution. *Sustain. Energy Fuels* **2020**, *4*, 5264–5270. [CrossRef]
10. Pati, P.B.; Damas, G.; Tian, L.; Fernandes, D.L.A.; Zhang, L.; Pehlivan, I.B.; Edvinsson, T.; Araujo, C.M.; Tian, H. An experimental and theoretical study of an efficient polymer nano-photocatalyst for hydrogen evolution. *Energy Environ. Sci.* **2017**, *10*, 1372–1376. [CrossRef]
11. Banerjee, T.; Gottschling, K.; Savasci, G.; Ochsenfeld, C.; Lotsch, B.V. H_2 evolution with covalent organic framework photocatalysts. *ACS Energy Lett.* **2018**, *3*, 400–409. [CrossRef] [PubMed]
12. Hug, S.; Mesch, M.B.; Oh, H.; Popp, N.; Hirscher, M.; Senker, J.; Lotsch, B.V. A fluorene based covalent triazine framework with high CO_2 and H_2 capture and storage capacities. *J. Mater. Chem. A* **2014**, *2*, 5928–5936. [CrossRef]
13. Lee, W.Y.; Cheng, K.F.; Wang, T.F.; Chueh, C.C.; Chen, W.C.; Tuan, C.S.; Lin, J.L. Effects of acceptors on the electronic and optoelectronic properties of fluorene-based donor–Acceptor–donor copolymers. *Macromol. Chem. Phys.* **2007**, *208*, 1919–1927. [CrossRef]
14. Guo, L.; Niu, Y.; Xu, H.; Li, Q.; Razzaque, S.; Huang, Q.; Jin, S.; Tan, B. Engineering heteroatoms with atomic precision in donor-acceptor covalent triazine frameworks to boost photocatalytic hydrogen production. *J. Mater. Chem. A* **2018**, *6*, 19775–19781. [CrossRef]
15. Bibi, S.; Bilal, S.; Ali Shah, A.U.H.; Ullah, H. Systematic analysis of poly(o-aminophenol) humidity sensors. *ACS Omega* **2017**, *2*, 6380–6390. [CrossRef] [PubMed]
16. Ullah, H.; Bibi, S.; Tahir, A.A.; Mallick, T.K. Donor-acceptor polymer for the design of all-solid-state dye-sensitized solar cells. *J. Alloys Compd.* **2017**, *696*, 914–922. [CrossRef]
17. Xiang, Y.; Wang, X.; Rao, L.; Wang, P.; Huang, D.; Ding, X.; Zhang, X.; Wang, S.; Chen, H.; Zhu, Y.; et al. Conjugated polymers with sequential fluorination for enhanced photocatalytic H_2 evolution via proton-coupled electron transfer. *ACS Energy Lett.* **2018**, *3*, 2544–2549. [CrossRef]
18. Bai, Y.; Woods, D.J.; Wilbraham, L.; Aitchison, C.M.; Zwijnenburg, M.A.; Sprick, R.S.; Cooper, A.I. Hydrogen evolution from water using heteroatom substituted fluorene conjugated co-polymers. *J. Mater. Chem. A* **2020**, *8*, 8700–8705. [CrossRef]
19. Frisch, M.J.; Trucks, G.W.; Schlegel, H.B.; Scuseria, G.E.; Robb, M.A.; Cheeseman, J.R.; Scalmani, G.; Barone, V.; Petersson, G.A.; Nakatsuji, H.; et al. *Gaussian 16 Revision*; Gaussian, Inc.: Wallingford, CT, USA, 2016.
20. Hanwell, M.D.; Curtis, D.E.; Lonie, D.C.; Vandermeersch, T.; Zurek, E.; Hutchison, G.R. Avogadro: An advanced semantic chemical editor, visualization, and analysis platform. *J. Cheminform.* **2012**, *4*, 17. [CrossRef]
21. Halgren, T.A. Merck molecular force field. I. Basis, form, scope, parameterization, and performance of MMFF94. *J. Comput. Chem.* **1996**, *17*, 490–519. [CrossRef]
22. Becke, A.D. A new mixing of hartree–fock and local density-functional theories. *J. Chem. Phys.* **1993**, *98*, 1372–1377. [CrossRef]
23. Franco, F.C.; Padama, A.A.B. DFT and TD-DFT study on the structural and optoelectronic characteristics of chemically modified donor-acceptor conjugated oligomers for organic polymer solar cells. *Polymer* **2016**, *97*, 55–62. [CrossRef]
24. Aicha Youssef, A.; Mohamed Bouzzine, S.; Mohyi Eddine Fahim, Z.; Sıdır, İ.; Hamidi, M.; Bouachrine, M. Designing donor-acceptor thienopyrazine derivatives for more efficient organic photovoltaic solar cell: A DFT study. *Phys. B Condens. Matter.* **2019**, *560*, 111–125. [CrossRef]

25. Lan, Z.A.; Ren, W.; Chen, X.; Zhang, Y.; Wang, X. Conjugated donor-acceptor polymer photocatalysts with electron-output "tentacles" for efficient hydrogen evolution. *Appl. Catal. B Environ.* **2019**, *245*, 596–603. [CrossRef]
26. Patra, B.C.; Khilari, S.; Manna, R.N.; Mondal, S.; Pradhan, D.; Pradhan, A.; Bhaumik, A. A metal-free covalent organic polymer for electrocatalytic hydrogen evolution. *ACS Catal.* **2017**, *7*, 6120–6127. [CrossRef]
27. Chen, B.S.; Chen, D.Y.; Chen, C.L.; Hsu, C.W.; Hsu, H.C.; Wu, K.L.; Liu, S.H.; Chou, P.T.; Chi, Y. Donor-acceptor dyes with fluorine substituted phenylene spacer for dye-sensitized solar cells. *J. Mater. Chem.* **2011**, *21*, 1937–1945. [CrossRef]
28. Afroz, M.A.; Sonigara, K.K.; Bhim Raju, T.; Soni, S.S.; Iyer, P.K. Effect of fluorine substitution and position on phenylene spacer in carbazole based organic sensitizers for dye sensitized solar cells. *Phys. Chem. Chem. Phys.* **2017**, *19*, 28579–28587. [CrossRef]
29. Ting, L.Y.; Jayakumar, J.; Chang, C.L.; Lin, W.C.; Elsayed, M.H.; Chou, H.H. Effect of controlling the number of fused rings on polymer photocatalysts for visible-light-driven hydrogen evolution. *J. Mater. Chem. A* **2019**, *7*, 22924–22929. [CrossRef]
30. Bai, Y.; Wilbraham, L.; Slater, B.J.; Zwijnenburg, M.A.; Sprick, R.S.; Cooper, A.I. Accelerated discovery of organic polymer photocatalysts for hydrogen evolution from water through the integration of experiment and theory. *J. Am. Chem. Soc.* **2019**, *141*, 9063–9071. [CrossRef]
31. Bredas, J.L. Mind the gap! *Mater. Horiz.* **2014**, *1*, 17–19. [CrossRef]